International Journal of Current Science Research and Review
ISSN: 2581-8341
Volume 08 Issue 01 January 2025
DOI: 10.47191/ijcsrr/V8-i1-30, Impact Factor: 7.943
IJCSRR @ 2025
www.ijcsrr.org

Analytical Modelling of Resistive Load Effect on Transient Voltage and Power Output from d_{33}-mode Piezoelectric Vibration Energy Harvester

Samuel E. Osheidu[1], Chigozie Israel-Cookey[2], Arobo R. C. Amakiri[3], Friday B. Sigalo[4], Onengiyeofori A. Davies[5*]

[1-5] Physics Department, Faculty of Science, Rivers State University, Port Harcourt, Rivers State, Nigeria

ABSTRACT: This research analytically investigates the effect of resistive load on the transient performance of a d_{33}-mode piezoelectric vibration energy harvester. Through normalized voltage and power analyses under varying normalized resistive loads and excitation frequencies, it is observed that the normalized voltage peaks consistently at resonance frequency, with its magnitude increasing as load resistance decreases. The normalized power, however, exhibits a maximum at an optimal load resistance that aligns with the system's internal impedance, underscoring the significance of impedance matching for efficient energy harvesting. Transient voltage and power dynamics reveal faster energy dissipation and higher fluctuations at lower resistances, while higher resistances yield smoother but less efficient energy transfer. These findings provide crucial insights into the interplay between load resistance, transient dynamics, and power optimization, paving the way for improved design and application of piezoelectric energy harvesters in real-world systems.

KEYWORDS: Piezoelectricity, Transient, Voltage, Power, Resistance

INTRODUCTION

The growing requirement for renewable energy sources to fulfill the world's energy needs has made the hunt for efficient and sustainable energy sources a central focus of contemporary scientific study. In this regard, a potential technique for transforming ambient mechanical vibrations into electrical energy is piezoelectric vibration energy harvesters, or PVEHs. According to Persano *et. al.* [1], the d_{33}-mode has drawn the most attention among the many piezoelectric topologies because of its improved electromechanical coupling efficiency and capacity to produce sizable charge outputs under mechanical stress. Applications like wireless sensor networks, biomedical implants, and wearable electronics that need for small, robust, and effective energy harvesting devices are especially well-suited for this mode of operation [2]. These applications frequently require stable energy sources that can operate independently of typical batteries, which are limited by finite lifespans and the logistical challenges of replacement.

While significant progress has been made in the modeling and optimization of PVEHs [2-4], much of the emphasis has been on steady-state performance, leaving key transient dynamics unexplored. During PVEH operation, the transient response—the period immediately after a change in external circumstances, such as the application of a load—is critical in determining the harvester's efficiency and dependability according to Poh and Naayagi [5]. The resistive load, an important element in energy harvesting systems, has a substantial impact on this transient behavior since it affects the pace of energy transfer as well as the development of voltage and power output [6]. Despite their relevance, the transient effects of resistive load fluctuations have not received adequate attention in existing analytical models, according to Brusa *et. al.* [7], which frequently assume idealized circumstances or steady-state operation. This knowledge gap hinders the capacity to build harvesters that can successfully adapt to dynamic and real-world operational situations.

The lack of comprehensive analytical models that account for the transitory impact of resistive loads on d_{33}-mode PVEHs is a significant concern [8]. Many practical applications rely on quick energy transfer during transient stages to ensure system operation. For example, in wireless sensor networks, a harvester may need to produce a burst of energy to commence transmission, but in biomedical devices, transient energy responses might have a direct impact on device performance and patient safety. Existing models, by ignoring or oversimplifying these transitory dynamics, fail to provide the accuracy and flexibility necessary for such applications.

This research aims to fill a significant knowledge gap by creating a strong analytical framework to model the impact of resistive loads on the transient voltage and power output of d_{33} piezoelectric vibration energy harvesters. The proposed model attempts to give a more in-depth knowledge of energy conversion processes under various load situations by capturing the interaction of electrical and

International Journal of Current Science Research and Review
ISSN: 2581-8341
Volume 08 Issue 01 January 2025
DOI: 10.47191/ijcsrr/V8-i1-30, Impact Factor: 7.943
IJCSRR @ 2025
www.ijcsrr.org

mechanical dynamics during the transient period. This study's insights are likely to help the construction of more efficient and adaptive energy harvesting devices, opening the door for breakthroughs in sectors that rely on autonomous, vibration-based power sources.

The significance of this research goes beyond its direct technical ramifications. This paper advances the theoretical knowledge of transitory effects in PVEHs, which contributes to the larger field of vibration-based energy harvesting. It establishes a framework for future research into similar transient phenomena in other piezoelectric setups and operational circumstances. Furthermore, the findings of this research should provide practical implications for the design of next-generation gadgets, improving their ability to function reliably in dynamic contexts. Finally, our study corresponds with the global push for sustainable and innovative energy solutions, reaffirming the importance of piezoelectric technology as a major enabler in the transition to a greener future.

MATHEMATICAL FORMULATION

Consider a single-degree- of- freedom (SDOF) mass-spring-damper-piezo encased in a rigid housing microgenerator system in which only a linear small displacement is allowed and is excited around its resonance frequency. Figure 1 shows a schematic representation of the piezoelectric vibration and the electromechanical model, *M* represents the equivalent rigid mass of the block, while x and y are the displacements of the base and the rigid mass under the external acceleration $\ddot{y}(t)$, *K* is the equivalent stiffness, and *C* is the mechanical loss coefficient (viscous damper) of the electromechanical model when all the piezoelectric elements are short-circuited. The electrical parameters $V = V_p$ and *I* are the output voltage and current of the piezoelectric elements connected in parallel, respectively.

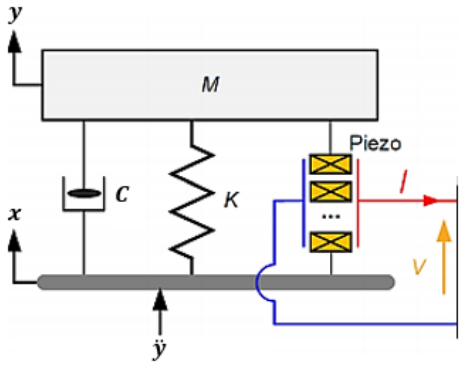

Figure 1. Schematic representation of SDOF piezoelectric and electromechanical coupling model [9]

Assuming that the difference between the base displacement *x* and the rigid mass displacement *y* is defined as the relative displacement $Z(t)$. Then, the dynamic equation of the electromechanical equation can be modelled using Newton's second law as [9-11]

$$M\ddot{Z}(t) + C\,\dot{Z}(t) + K\,Z(t) - \alpha\,V_p = -M\,\ddot{y}(t) \quad (1)$$

Where, the dot over the variable denotes differentiation with respect to time. Furthermore, assume a harmonic vibration excitation of the form $y(t) = F_0\,Sin(\omega t)$, where ω is the excitation frequency and F_0 is the amplitude and that the electromechanical coupling is very weak and negligible. Under these assumptions, the governing equation (2) becomes [12, 13],

$$M\ddot{Z}(t) + 2\xi\omega_n\,\dot{Z}(t) + {\omega_n}^2\,Z(t) = F_0\,\omega^2 Sin(\omega t) \quad (2)$$

With initial conditions,

$$Z(0) = 0, \quad \dot{Z}(0) = 0 \quad (3)$$

Where $\omega_n \left(= \sqrt{\frac{K}{M}}\right)$ is the natural frequency and $\xi = \frac{C}{2M\omega_n}$ is the damping ratio. Introducing the following dimensionless variables,

$$z = \frac{Z}{F_0}\ , \ \tau = t\omega_n,\ \Omega = \frac{\omega}{\omega_n} \quad (4)$$

The governing equation (2) and the initial conditions (3) reduce to the dimensionless forms,

$$\ddot{z}(\tau) + 2\xi\dot{z}(\tau) + z(\tau) = \Omega^2 \sin(\Omega\tau) \quad (5)$$

International Journal of Current Science Research and Review
ISSN: 2581-8341
Volume 08 Issue 01 January 2025
DOI: 10.47191/ijcsrr/V8-i1-30, Impact Factor: 7.943
IJCSRR @ 2025
www.ijcsrr.org

$$z(0) = 0, \quad \dot{z}(0) = 0 \tag{6}$$

Where Ω is the normalized frequency. The solution of equation (5) is of the form,

$$z(t) = z_c(\tau) + z_P(\tau) \tag{7}$$

Where $z_c(\tau)$ and $z_P(\tau)$ are the complimentary function and particular solution, respectively. The nonhomogeneous differential equation (5) has a complimentary solution, $z_c(\tau)$ of the form

$$z_c(\tau) = e^{-\xi\tau}(c_1 \cos(\beta\tau) + c_2 \sin(\beta\tau)) \tag{8}$$

Where $\beta = \sqrt{1-\xi^2}$, and c_1, c_2 are arbitrary constants which can be calculated from the initial conditions. Assume the particular solution, $z_p(\tau)$ of the form,

$$z_c(\tau) = e^{-\xi\tau}(c_1 \cos(\beta\tau) + c_2 \sin(\beta\tau)) \tag{9}$$

By setting $z(\tau) = z_p(\tau)$ in (5), substituting twice the differentiation of the resulting equation, and simplifying yield the following matrix equation

$$\begin{pmatrix} 1-\Omega^2 & -2\xi\Omega \\ 2\xi\Omega & 1-\Omega^2 \end{pmatrix}\begin{pmatrix} A \\ B \end{pmatrix} = \begin{pmatrix} \Omega^2 \\ 0 \end{pmatrix} \tag{10}$$

Solving the matrix equation (10) by applying the Crammer's method yield the solutions for *A* and *B* as

$$A = \frac{(1-\Omega^2)\Omega^2}{(1-\Omega^2)^2 + (2\xi\Omega)^2} \tag{11}$$

$$B = \frac{-2\xi\Omega^3}{(1-\Omega^2)^2 + (2\xi\Omega)^2} \tag{12}$$

Hence, the particular solution is

$$\begin{aligned} z_p(\tau) &= \frac{1}{[(1-\Omega^2)^2 + (2\xi\Omega)^2]}[(1-\Omega^2)\Omega^2 sin(\Omega\tau) - 2\xi\Omega^3 cos(\Omega\tau)] \\ &= \frac{sin(\Omega\tau)(1-\Omega^2)\Omega^2}{\sqrt{(1-\Omega^2)^2 + (2\xi\Omega)^2}} - \frac{cos(\Omega\tau)2\xi\Omega^3}{\sqrt{(1-\Omega^2)^2 + (2\xi\Omega)^2}} \\ \Rightarrow z_p(\tau) &= \frac{\Omega^2}{\sqrt{(1-\Omega^2)^2 + (2\xi\Omega)^2}}[\frac{sin(\Omega\tau)(1-\Omega^2)\Omega^2}{\sqrt{\Omega^2(1-\Omega^2)^2 + (2\xi\Omega)^2}} - \frac{cos(\Omega\tau)(2\xi\Omega^3)}{\sqrt{\Omega^2(1-\Omega^2)^2 + (2\xi\Omega)^2}}] \end{aligned} \tag{13}$$

Applying the trigonometric identity $Sin\,(a-b) = Sin\,(a)Cos\,(b) - Cos(a)Sin\,(b)$, equation (13) reduces to

$$z_p(\tau) = \Gamma[sin(\Omega\tau - \varphi)] \tag{14}$$

Where,

$$\Gamma = \Omega^2[(1-\Omega^2)^2 + (2\xi\Omega)^2]^{-1/2} \tag{15}$$

With the phase angle expressed as,

$$\varphi = \tan^{-1}\left(\frac{2\xi\Omega}{1-\Omega^2}\right) \tag{16}$$

Combing the results of the complementary and particular solution yield the complete solution of the normalized displacement of the system as,

$$z(\tau) = e^{-\xi\tau}(c_1 \cos(\beta\tau) + c_2 \sin(\beta\tau)) + \Gamma[sin(\Omega\tau - \varphi)] \tag{17}$$

The solution of equation (17) consists of two parts, where the first part represents the transient response, the second part represents the steady – state response of the system. To proceed with analysis, assume that the transient solution of the normalized displacement, $z_c(\tau)$, dies quickly as τ increases under preloaded piezoelectric system [14]. Under the above assumption, the normalized relative displacement reduces to a steady state harmonic, $z(\tau)$ which continue indefinitely. Thus, the displacement, $z(\tau)$, and the magnitude of the acceleration, $a(\tau)$, is defined as,

$$z(\tau) = \Gamma[sin(\Omega\tau - \varphi)] \tag{18}$$

$$a(\tau) = |\ddot{z}(\tau)| = \Omega^2\Gamma sin(\Omega\tau - \varphi) \tag{19}$$

International Journal of Current Science Research and Review
ISSN: 2581-8341
Volume 08 Issue 01 January 2025
DOI: 10.47191/ijcsrr/V8-i1-30, Impact Factor: 7.943
IJCSRR @ 2025
www.ijcsrr.org

In order to consider the effect of resistive load on the voltage and power outputs of the piezoelectric device, we assume that the piezoelectric patch is poling in direction 3. Hence, the constitutive equation for the surface charge displacement of the PZT material generated by the normal stress induced deformation is given by [15],

$$D_3(t) = d_{33}\, T_3(t) + \varepsilon_{33}\, E_3(t) \tag{20}$$

Where d_{33} is the piezoelectric charge coefficient with induced polarization in direction 3 per unit stress applied in direction 3, ε_{33} is the permittivity constant, $E_3(t)$ is the electric field in direction 3 and $T_3(t)$ is the normal stress along direction 3.

Now, the strength of the electric patch is dominated by the voltage difference, $V_p(t)$ across the piezoelectric layer and is given by [15, 16],

$$E_3(t) = -\frac{V_p(t)}{h} \tag{21}$$

Where $V_p(t)$ is the output voltage between the ends of the piezoelectric layer and h is the thickness of the piezoelectric layer. According to Li *et al.* [13], the stress in direction 3 is given by,

$$T_3(t) = \frac{F(t)}{A} = -\frac{nd_{33}KZ(t)}{A} \tag{22}$$

Where $F(t)$ is the force exerted on the spring is related to the displacement, $Z(t)$ and by Hooke's law, $F(t) = -KZ(t)$, K is the stiffness of the spring, n is the total number of all the patches and A is the total area of all the piezoelectric layers in the patches. The substitution of Equations (21) and (22) into Equation (20) gives

$$D_3(t) = -\frac{nd_{33}KZ(t)}{A} - \varepsilon_{33}\frac{V_p(t)}{h}$$

$$\Rightarrow V_p(t) + \frac{hD_3(t)}{A\varepsilon_{33}} + \frac{nd_{33}KZ(t)}{A\,\varepsilon_{33}} = 0 \tag{23}$$

Differentiating Equation (23) with respect to time, t yields,

$$\dot{V}_p(t) + \frac{h}{A\varepsilon_{33}}\,\dot{D}_3(t) + \frac{nd_{33}K}{A\,\varepsilon_{33}}\,\dot{Z}(t) = 0 \tag{24}$$

On simplifying further gives the following first order linear differential equation,

$$\dot{V}(t) + \frac{V_p(t)}{c_P R} + \frac{nd_{33}K}{c_p}\,\dot{Z}(t) = 0 \tag{25}$$

Where $c_p = \frac{\varepsilon_{33A}}{h} = \frac{k_{33}^T\varepsilon_0 A}{h}$ is the capacitance of the piezoelectric material and the output voltage in the piezoelectric harvester across the total load resistance is given by$V_p(t) = RA\dot{D}_3(t)$ [17]. Also, $k_{33}^T\varepsilon_0$ is the relative dielectric constant of the piezoelectric material and $\varepsilon_0 = 8.85 \times 10^{-12}$ is the permittivity constant of the free space.

By defining the following dimensionless variables,

$$z = Z, v = \frac{c_p}{d_{33}K}V_p, \tau = \omega_n t \tag{26}$$

Equation (25) becomes,

$$\dot{v}(\tau) + \frac{1}{R_N}v(\tau) = -\Omega\,\Gamma Cos(\Omega\tau - \varphi) \tag{27}$$

Where $z = \Gamma\ \mathrm{Sin}\ (\Omega\tau - \varphi)$ and $R_N = \omega_n c_P R$ is the normalized electrical resistance. The initial condition for equation (27) is,

$$v(0) = 0 \tag{28}$$

Equation (27) subject to initial conditions is a well-known first order linear differential equation whose solution is well known. By adopting an integrating factor, $\mu(\tau)$ given by

$$\mu(\tau) = Exp\left[\int \frac{1}{R_N}\right]d\tau = Exp\left[\frac{\tau}{R_N}\right] \tag{29}$$

Multiplying both sides of equation (29) and integrating gives the output voltage of the system as

$$v(\tau) = c_1 e^{-\tau/R_N} - \frac{\Omega\,\Gamma\,R_N^2}{R_N(1 + R_N^2\,\Omega^2)}(Cos(\Omega\tau - \varphi) - R_N\Omega\ \mathrm{Sin}(\Omega\tau - \varphi)) \tag{30}$$

Applying the initial condition (30) gives,

International Journal of Current Science Research and Review
ISSN: 2581-8341
Volume 08 Issue 01 January 2025
DOI: 10.47191/ijcsrr/V8-i1-30, Impact Factor: 7.943
IJCSRR @ 2025
www.ijcsrr.org

$$c_1 = \frac{\Omega\,\Gamma\,R_N}{(1 + R_N^2\,\Omega^2)}(Cos(\varphi) + R_N\Omega\,\mathrm{Sin}(\varphi)) \tag{31}$$

Therefore, the output voltage, $v(\tau)$ is,

$$v(\tau) = \Gamma_1\left(e^{-\frac{\tau}{R_N}}\,Sin(\theta + \varphi) - \mathrm{Sin}(\Omega\tau + \theta - \varphi)\right) \tag{32}$$

Where, $\Gamma = \Omega^2((1-\Omega^2)^2 + (2\xi\Omega)^2)^{-1/2}$, $\Gamma_1 = \frac{\Omega\,\Gamma\,R_N}{(1+R_N^2\,\Omega^2)}$, $\varphi = Tan^{-1}\left(\frac{2\xi\Omega}{1-\Omega^2}\right)$ and $\theta = Tan^{-1}\left(\frac{1}{R_N\Omega}\right)$. For the purpose of the computations, the dimensions of d_{33} Piezo-ceramic disc for PZT 4, PZT 5A and PZT 5H are computed using the given equation;

$$c_P = \frac{\varepsilon_{33A}}{h} = \frac{k_{33}^T\varepsilon_0 A}{h} \tag{33}$$

By definition, the normalized output power, $p(\tau)$, will be defined as,

$$p(\tau) = \frac{[v(\tau)]^2}{R_N} \tag{34}$$

The dimensions and properties of the ceramic discs used in this work are summarized in Table 1 below:

Table 1: Dimensions and Properties of PZT 4, PZT 5A and PZT 5H (Boston Piezo-Optics, Inc, (2023)

Parameters	PZT 4	PZT 5A	PZT 5H
Diameter of disc (mm)	47.33	41.40	29.27
Thickness of disc, h (mm)	0.6	0.6	0.6
Number of layers, n	80	80	80
k_{33}^T	1300	1700	3400
$d_{33}\ (\times 10^{-12}\ \frac{C}{N})$	289	374	593
$\varepsilon_0(\times 10^{-12}\ \frac{F}{m})$	8.854	8.854	8.854
Capacitance, $C_p\ (\mu F)$	2.7	2,7	2.7

RESULTS

Estimates of θ, ψ and ξ produced values of 1.5, 0.13 and 0.03 respectively. After modelling for the output normalized voltage and normalized power using these estimates, plots of normalized voltage and normalized power against normalized frequency and normalized frequency for varying measures of normalized load resistance (1.05, 3.14 and 10.47). These results are shown in Figures 2 to 3..

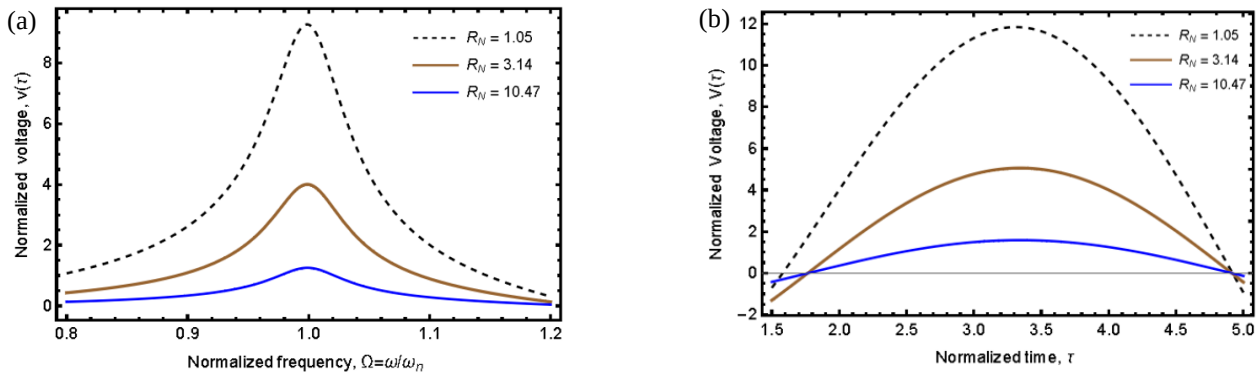

Figure 2: (a) Normalized voltage against normalized frequency for varying normalized load resistance (b) Normalized voltage against normalized time for varying normalized load resistance

International Journal of Current Science Research and Review
ISSN: 2581-8341
Volume 08 Issue 01 January 2025
DOI: 10.47191/ijcsrr/V8-i1-30, Impact Factor: 7.943
IJCSRR @ 2025
www.ijcsrr.org

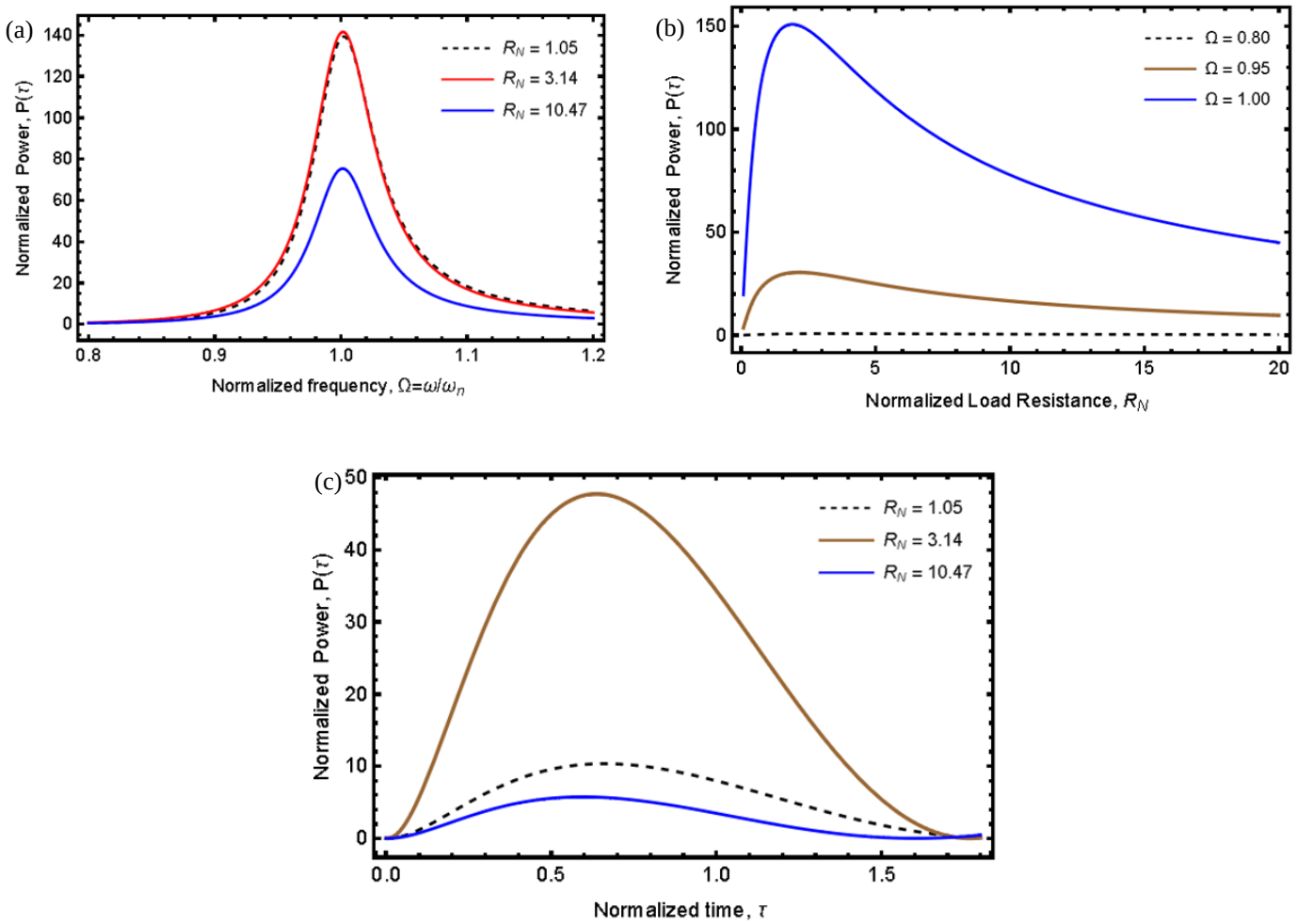

Figure 3: (a) Normalized power against normalized frequency for varying normalized load resistance (b) Normalized power against normalized load resistance for varying normalized frequency (c) Normalized power against normalized time for varying normalized load resistance

DISCUSSION

In any piezoelectric harvesting system, resonance occurs when the natural frequency of the piezoelectric element matches the frequency of the external vibration source [18, 19]. At this point, the system experiences maximum amplitude of vibration leading to enhanced energy conversion and improved power output. Examining the plot of normalized voltage against normalized frequency for varying normalized load resistance, as seen in Figure 2a, it is immediately obvious that the normalized voltage peaks at the resonance normalized frequency (1 in this case) irrespective of the load resistance, with the magnitude of the voltage increasing with decreasing load resistance. This could be indicative of the fact that the system's response is dominated by its intrinsic resonance dynamics, with improved energy transfer and voltage output at lower resistances, according to Zhou *et. al.* [20].

Further analysing the plot of normalized voltage against normalized time for varying normalized load resistance (Figure 2b), it can be observed that the transient voltage response exhibits damped oscillations that settle to a steady-state value over time, with the settling time and peak amplitudes depending on the load resistance. Evidently, for lower normalized load resistances, the voltage amplitude and decay rate are higher, which could be indicative of faster energy dissipation and reduced electrical damping as suggested by Touairi and Mabrouki [21]. Conversely, for higher resistances, the voltage oscillations are more sustained and decay slower, suggestive of increased electrical damping and less immediate energy transfer to the load. In other words, the resistive load

International Journal of Current Science Research and Review
ISSN: 2581-8341
Volume 08 Issue 01 January 2025
DOI: 10.47191/ijcsrr/V8-i1-30, Impact Factor: 7.943
IJCSRR @ 2025
www.ijcsrr.org

affects the energy dissipation rate and the dynamic response of the piezoelectric harvester, with lower resistance facilitating rapid energy transfer at the cost of increased transient oscillations, while higher resistance stabilizes the output but limits the energy extraction rate.

Additionally, the plot of normalized power against normalized frequency for varying normalized load resistance, as seen in Figure 3a, shows that the normalized power reaches a peak at the resonance frequency for all load resistances, with its amplitude varying across resistance values. However, as the normalized load resistance decreases, the amplitude of the power generally increases initially, reaching a maximum at an optimal load resistance, beyond which further decreases in resistance cause the power to drop. This behavior reflects the impedance matching principle, where maximum power transfer occurs when the load resistance matches the internal electrical impedance of the piezoelectric harvester [22, 23]. Therefore, it can be seen that optimal power output depends on tuning the load resistance to balance energy transfer efficiency and the dissipation rate, with deviations from the optimal resistance reducing the harvested power.

Furthermore, analysing the plot of normalized power against normalized load resistance for varying normalized frequency (Figure 3b) it can be observed that at the resonance frequency (1 in this case), the power output exhibits a peak at an optimal load resistance, with the peak diminishing as the frequency deviates from resonance. Evidently, as frequencies deviates from resonance, the power output decreases, and the peak becomes less pronounced, indicating reduced energy transfer efficiency. In other words, maximum power output is achieved when the load resistance is optimally matched to the system's impedance at resonance, and deviations from this resistance or frequency reduce the energy harvesting efficiency due to impedance mismatch or diminished mechanical-electrical coupling [22].

Finally, a plot of normalized power against normalized time for varying normalized load resistance (Figure 3c) was analysed. It is observed that the power initially exhibits transient oscillations before stabilizing to a steady-state value, with the settling time and peak power influenced by the load resistance. For lower load resistance, the transient power has a higher peak, however decays faster due to rapid energy dissipation [24], whereas higher load resistance results in slower power stabilization and lower steady-state power due to reduced energy transfer efficiency [25]. Therefore, load resistance affects both the transient dynamics and steady-state power output, with lower resistance enabling faster energy extraction at the cost of transient fluctuations and higher resistance providing smoother but less efficient energy harvesting. Additionally, it can be seen that the power peaks at an optimal load resistance, dropping below or above this optimal value. This verifies our previous findings as the system's power output is maximized when the load resistance is matched to the system's internal impedance, with deviations from this optimal resistance resulting in reduced power due to impedance mismatch and less efficient energy transfer.

CONCLUSION

This study analytically investigated the effects of resistive load on the transient voltage and power dynamics of a d_{33}-mode piezoelectric vibration energy harvester. Key findings reveal that the normalized voltage consistently peaks at the resonance frequency irrespective of load resistance, while its magnitude increases as load resistance decreases. The power output, however, exhibits a clear dependency on the resistive load, peaking at an optimal load resistance that matches the system's internal impedance, highlighting the importance of impedance matching for maximum energy transfer. Analysis of transient behaviour shows that lower resistive loads facilitate rapid energy dissipation with higher transient fluctuations, whereas higher resistances stabilize the output at the cost of reduced energy transfer efficiency. These results provide a framework for optimizing load resistance to maximize energy harvesting performance, balancing steady-state power output with transient dynamics. Future work could explore the impact of non-linear effects, environmental variations, and multi-frequency excitations to enhance the robustness of piezoelectric energy harvesting systems.

REFERENCES

1. Persano, L., A. Camposeo, F. Matino, R. Wang, T. Natarajan, Q. Li, M. Pan, Y. Su, S. Kar-Narayan, and F. Auricchio, *Advanced materials for energy harvesting and soft robotics: Emerging frontiers to enhance piezoelectric performance and functionality.* Advanced Materials, 2024. 36(45): p. 2405363.
2. Oki, P., C. Israel-Cookey, A.R. Amakiri, O.A. Davies, P.A. Ngeri, and N.N. Tasie, *Mathematical modelling of Shoe-Mounted-Mode Piezoelectric Energy Harvesting System.* International Journal of Scientific Research and Engineering Development, 2024. 7(6): p. 244-259.

3. Umegaki, T. and I. Kanno, *Structural optimization of piezoelectric thin-film vibration energy harvesters based on electric equivalent circuit model*, in *Nanoscale Ferroelectric-Multiferroic Materials for Energy Harvesting Applications*. 2019, Elsevier. p. 161-179.
4. Liang, H., G. Hao, and O.Z. Olszewski, *A review on vibration-based piezoelectric energy harvesting from the aspect of compliant mechanisms.* Sensors and Actuators A: Physical, 2021. 331: p. 112743.
5. Poh, W.Q.T. and R. Naayagi. *Modelling and Integration of a Piezoelectric Cantilever Beam with Quasi-Z-Source Inverter for Self-Powered Dynamic System Application*. in *2020 IEEE Power & Energy Society General Meeting (PESGM)*. 2020. IEEE.
6. Wu, N., B. Bao, and Q. Wang, *Review on engineering structural designs for efficient piezoelectric energy harvesting to obtain high power output.* Engineering Structures, 2021. 235: p. 112068.
7. Brusa, E., A. Carrera, and C. Delprete, *Integrated mechatronic design of an industrial piezoelectric vibration energy harvester.* Mechanics of Advanced Materials and Structures, 2024. 31(27): p. 8966-8980.
8. Brusa, E., A. Carrera, and C. Delprete. *A Review of Piezoelectric Energy Harvesting: Materials, Design, and Readout Circuits*. in *Actuators*. 2023. MDPI.
9. Guyomar, D., A. Badel, E. Lefeuvre, and C. Richard, *Toward energy harvesting using active materials and conversion improvement by nonlinear processing.* IEEE transactions on Ultrasonics, Ferroelectrics and Frequency Control, 2005. 52(4): p. 584-595.
10. Wu, Y., Q. Yuan, K. Ren, X. Shen, H. Shen, A. Badel, H. Ji, and J. Qiu, *Bidirectional energy-controlled piezoelectric shunt damping technology and its vibration attenuation performance.* International Journal of Mechanical System Dynamics, 2024. 4(1): p. 63-76.
11. Brenes, A., A. Morel, J. Juillard, E. Lefeuvre, and A. Badel, *Maximum power point of piezoelectric energy harvesters: A review of optimality condition for electrical tuning.* Smart Materials and Structures, 2020. 29(3): p. 033001.
12. Gatti, G., M. Brennan, M. Tehrani, and D. Thompson, *Harvesting energy from the vibration of a passing train using a single-degree-of-freedom oscillator.* Mechanical Systems and Signal Processing, 2016. 66: p. 785-792.
13. Li, Y., D. Yin, X. Cheng, J. Chen, A. Zhou, X. Ji, and Y. Li, *Vibration energy harvesting with piezoelectric ceramics working in d33 mode by using a spring-mass-spring oscillator.* Journal of Applied Physics, 2020. 127(6).
14. Zhang, B., H. Liu, D. Li, J. Liang, and J. Gao, *Analytical modeling and validation of a preloaded piezoceramic current output.* Micromachines, 2021. 12(4): p. 353.
15. Xiao, Y., Q. Ji, S. Karnaoukh, C. Wang, and N. Wu, *Design and analysis of a d33 mode piezoelectric energy generator for vehicle braking system.* Smart Materials and Structures, 2022. 31(6): p. 065027.
16. Qian, F., T.-B. Xu, and L. Zuo, *Design, optimization, modeling and testing of a piezoelectric footwear energy harvester.* Energy Conversion and Management, 2018. 171: p. 1352-1364.
17. Feenstra, J., J. Granstrom, and H. Sodano, *Energy harvesting through a backpack employing a mechanically amplified piezoelectric stack.* Mechanical Systems and Signal Processing, 2008. 22(3): p. 721-734.
18. Song, H.C., S.W. Kim, H.S. Kim, D.G. Lee, C.Y. Kang, and S. Nahm, *Piezoelectric energy harvesting design principles for materials and structures: material figure-of-merit and self-resonance tuning.* Advanced Materials, 2020. 32(51): p. 2002208.
19. Wu, Y., S. Li, K. Fan, H. Ji, and J. Qiu, *Investigation of an ultra-low frequency piezoelectric energy harvester with high frequency up-conversion factor caused by internal resonance mechanism.* Mechanical Systems and Signal Processing, 2022. 162: p. 108038.
20. Zhou, W., D. Du, Q. Cui, Z. Yang, C. Lu, Y. Wang, and Q. He, *Piezoelectric vibration energy harvester: Operating mode, excitation type and dynamics.* Advances in Mechanical Engineering, 2022. 14(10): p. 16878132221131177.
21. Touairi, S. and M. Mabrouki, *Chaotic dynamics applied to piezoelectric harvester energy prediction with time delay.* International Journal of Dynamics and Control, 2021. 10: p. 699–720.
22. Liao, Y. and J. Liang, *Maximum power, optimal load, and impedance analysis of piezoelectric vibration energy harvesters.* Smart Materials and Structures, 2018. 27(7): p. 075053.

International Journal of Current Science Research and Review
ISSN: 2581-8341
Volume 08 Issue 01 January 2025
DOI: 10.47191/ijcsrr/V8-i1-30, Impact Factor: 7.943
IJCSRR @ 2025
www.ijcsrr.org

23. Liang, J. and W.-H. Liao, *Impedance modeling and analysis for piezoelectric energy harvesting systems.* IEEE/ASME Transactions on Mechatronics, 2011. 17(6): p. 1145-1157.
24. Li, X., K. Liu, L. Xiong, and L. Tang, *Development and validation of a piecewise linear nonlinear energy sink for vibration suppression and energy harvesting.* Journal of Sound and Vibration, 2021. 503: p. 116104.
25. Xiong, L., L. Tang, K. Liu, and B.R. Mace, *Broadband piezoelectric vibration energy harvesting using a nonlinear energy sink.* Journal of Physics D: Applied Physics, 2018. 51(18): p. 185502.

Cite this Article: Samuel E. Osheidu, Chigozie Israel-Cookey, Arobo R. C. Amakiri, Friday B. Sigalo, Onengiyeofori A. Davies (2025). Analytical Modelling of Resistive Load Effect on Transient Voltage and Power Output from d_33-mode Piezoelectric Vibration Energy Harvester. International Journal of Current Science Research and Review, 8(1), 278-286, DOI: https://doi.org/10.47191/ijcsrr/V8-i1-30